High-resolution resonance photoemission study of CeMX (M=Pt, Pd; X=P, As, Sb)

T. Iwasaki, A. Sekiyama, A. Yamasaki, M. Okazaki, K. Kadono, H. Utsunomiya, and S. Imada
Division of Materials Physics, Graduate School of Engineering Science, Osaka University, Toyonaka, Osaka 560-8531, Japan

Y. Saitoh
Japan Atomic Energy Research Institute, SPring-8, Mikazuki, Hyogo 679-5148, Japan

T. Muro and T. Matsushita
Japan Synchrotron Radiation Research Institute, SPring-8, Mikazuki, Hyogo 679-5198, Japan

H. Harima
The Institute of Scientific and Industrial Research, Osaka University, Ibaraki 567-0047, Japan

S. Yoshii* and M. Kasaya
Department of Physics, Tohoku University, Sendai 980-8578, Japan

A. Ochiai
Center for Low Temperature Science, Tohoku University, Sendai 980-8578, Japan

T. Oguchi
Department of Physics, Hiroshima University, Higashi-Hiroshima 739-8526, Japan

K. Katoh and Y. Niide
School of Applied Sciences, National Defense Academy, Yokosuka 239-8686, Japan

K. Takegahara
Department of Materials Science and Technology, Hirosaki University, Hirosaki 036-8561, Japan

S. Suga
Division of Materials Physics, Graduate School of Engineering Science, Osaka University, Toyonaka, Osaka 560-8531, Japan
(Received 22 March 2001; revised manuscript received 25 October 2001; published 23 April 2002)

We have performed high-resolution Ce $3d$-$4f$ resonance photoemission (RPES) measurements for low Kondo temperature (T_K) CeMX (M=Pd,Pt,X=P,As,Sb) and compared the results with $4d$-$4f$ RPES. The experimental results reveal that the bulk Ce $4f$ electronic structures are remarkably different from those in the surface layer even in low-T_K materials. The non-$4f$ valence-band spectra are well described by the results of the band-structure calculation of isostructural LaMX by considering the photoionization cross sections. We have analyzed the Ce $4f$ spectra by using a noncrossing approximation calculation based on the single-impurity Anderson model. The calculated results successfully reproduce the experimental $4f$ spectra. We find that the bare $4f$ level shift is the most important factor in explaining the difference between the surface and bulk Ce $4f$ spectra. Moreover, the Ce $4f$ states of CeMX are found to hybridize preferentially with a particular part of the *p-d* mixed antibonding states.

DOI: 10.1103/PhysRevB.65.195109 PACS number(s): 79.60.−i, 71.20.Eh, 72.15.Qm

I. INTRODUCTION

In Ce compounds, their physical properties are strongly influenced by the Ce $4f$ electronic structures. High-energy spectroscopic measurements such as photoemission spectroscopy (PES), inverse photoemission spectroscopy, and x-ray absorption spectroscopy are very useful in investigating the nature of the Ce $4f$ states.[1] However, experimental PES spectra of most Ce compounds contain overlapping contributions from both $4f$ and valence-band states, which are often difficult to be disentangled. Resonance photoemission spectroscopy (RPES), using synchrotron radiation, is very effective in revealing the $4f$ components.[2] A widely used Ce $4d$-$4f$ RPES ($h\nu \sim 122$ eV) has an advantage of good energy resolution ($\Delta E \sim 40$ meV) that enables one to observe such fine structures in the vicinity of the Fermi level (E_F) as a tail of the Kondo resonance, its crystal field excitation (<60 meV), and its spin-orbit splitting sideband (~ 300 meV).[3,4] However, Laubschat *et al.* first reported that the "bulk-sensitive" Ce $3d$-$4f$ RPES spectra ($h\nu \sim 882$ eV) were much different from those of the $4d$-$4f$ RPES,[5] suggesting that the Ce $4f$ electronic structures in the surface region were remarkably different from those in the bulk region. Their results mean that the Ce $4d$-$4f$ RPES spectra heavily contain the surface contributions due to the short mean free path of the excited electron (<5 Å) and the $4d$-$4f$

RPES has a flaw in probing bulk electronic structures. Thereafter, several works have been done for the bulk/surface Ce $4f$ problem by using both the ''bulk-sensitive'' Ce $3d$-$4f$ and ''surface-sensitive'' $4d$-$4f$ RPES.[6–12] However, the energy resolution ($\Delta E \sim 0.7$ eV) of the employed Ce $3d$-$4f$ RPES measurement in these works was not sufficient to resolve such fine structures near E_F. Thus, it has been difficult to give detailed discussions on the difference between the surface and bulk $4f$ electronic states. A very recent development in high-brilliance synchrotron radiation source and advanced instrumentation enables us to perform Ce $3d$-$4f$ RPES with sufficient total energy resolution ($\Delta E \sim 100$ meV).[13] Now, we can perform the high-resolution ''bulk-sensitive'' $3d$-$4f$ RPES and compare the results with ''surface-sensitive'' $4d$-$4f$ RPES measurements for Ce compounds and quantitatively discuss the difference between the bulk and surface $4f$ electronic structures.[14–17]

In this study, we focus on ternary Ce pnictide compounds, CeMX (M=Pd,Pt,X=P,As,Sb), which are well known to exhibit various unusual properties. The *p-f* hybridization between semimetallic pnictogen *p* bands and Ce $4f$ states plays an important role in their electronic structures in the valence-band region, in particular in the vicinity of E_F.[18–20] The present CeMX samples belong to very weakly hybridized systems with the Kondo temperature (T_K)$\leqslant$1 K. CePtP shows successive phase transitions from the ferromagnetic ordering at T_C=3.1 K and the antiferromagnetic ordering at T_N=0.9 K.[21] The easy axis of CePtP lies along the *c* axis while the electric conductivity in the *c* plane is better than that along the *c* axis. CePtAs also shows anisotropy along the *c* axis in the electric resistivity but the magnetic anisotropy is not clearly observed,[22,23] although the antiferromagnetic ordering occurs in CePtAs at around 1.0 K.

CePdP is a new material that exhibits a ferromagnetic ordering at 5.2 K. Although CePdAs was reported to show antiferromagnetic ordering at around $T_N \sim 4$ K in the previous work,[24] a recent study by Katoh *et al.* reveals that it has a ferromagnetic ground state with $T_C \sim 6.2$ K. CePdSb has a ferromagnetic ground state with a relatively high ordering temperature T_C=17.5 K.[25] The easy axes of these three reported CePdX compounds are found to lie in the *c* plane.

CeMX are two-dimensional layered compounds, composed of the Ce layer and the *M*-*X* layer piled up along the *c* axis. Most compounds show the anisotropy in the electric resistivity and the magnetic susceptibility. The crystal structures of both CePdP and CePdAs are hexagonal ZrBeSi type with the Pd and P (or As) atoms in the same plane. CePdSb and CePtSb have hexagonal LiGaGe-type crystal structure, where the Pd and Sb atoms form puckered layers. Both CePtP and CePtAs have the hexagonal YPtAs-type structure, in which the unit cell of the LiGaGe type is heaped on another unit cell, rotated by 60° around the *c* axis. Therefore, the YPtAs-type structure has two Ce sites with the trigonal (Ce I) and hexagonal symmetry (Ce II).

In this paper, we present high-resolution Ce $3d$-$4f$ and $4d$-$4f$ RPES results for CeMX. We compare the non-$4f$ valence-band spectra taken at the resonance minimum ($3d$-$4f$: $h\nu$=875 eV and $4d$-$4f$: $h\nu$=114 eV) with the band-structure calculations of isostructural LaMX and quantitatively discuss the electronic structures of the valence bands.[26,27] Then, we analyze the Ce $4f$ spectra by using the noncrossing approximation (NCA) calculation[28–30] based on the single-impurity Anderson model (SIAM).[31,32] We quantitatively discuss the difference between the bulk and surface electronic structures of Ce $4f$ states and their substitution dependence.

II. EXPERIMENT

The single-crystal samples of CeMX (M=Pd,Pt,X=P,As,Sb) were prepared by the Bridgman method in evacuated tungsten crucibles sealed by electron beam welding. Ce $3d$-$4f$ RPES measurements were carried out at BL-25SU of SPring-8,[13] whereas the Ce $4d$-$4f$ RPES measurements were performed at BL-3B of the Photon Factory, High Energy Accelerator Research Organization,[33] by using the GAMMADATA-SCIENTA SES-200 hemispherical electron analyzer. We carried out the $3d$-$4f$ RPES measurements with improved energy resolution of ~100 meV full width at half maximum (FWHM) compared with the previous work.[34] The FWHM was about 50 meV for the $4d$-$4f$ RPES study. The samples were cooled down to 20 K. The clean surfaces were obtained by *in situ* repeated scraping until no contamination could be detected in the photoemission regions of the O $1s$, C $1s$ (for $3d$-$4f$ RPES minimum), and O $2p$ (for $4d$-$4f$ RPES minimum) signals. The base pressure was $\sim 4\times10^{-10}$ Torr during the measurements.

III. RESULTS AND DISCUSSION

A. Resonance photoemission spectra

The $3d$-$4f$ core absorption spectra were first measured with high resolution. Then the RPES spectra were measured at different photon energies. The spectra were rather similar to that of CePdSn.[35] The RPES Ce $4f$ spectral shape depends slightly upon the excitation photon energy as seen in Fig. 2 of this reference. However, the differences in the cases of CePtX and CePdX are not very large compared with the difference between the $3d$-$4f$ and $4d$-$4f$ RPES. Therefore, the on-resonance spectra measured at the higher-energy peak (~882 eV) of the main absorption band are shown in this manuscript. The left panels of Fig. 1 show the $4f$ components for CePtP (upper panel) and CePtAs (lower panel). The shaded spectra represent the ''bulk-sensitive'' $3d$-$4f$ RPES spectra, whereas the dashed curves show the ''surface-sensitive'' $4d$-$4f$ spectra. All spectra are normalized to the same area after the subtraction of the integral-type background from the raw spectra. The $4f$ spectra are then obtained by subtracting the non-$4f$ spectra (resonance-minimum spectra, whose shapes are given in the right panels but their intensities are much weaker as shown later) from the resonance-maximum spectra. The $4f$ spectra of these compounds consist of two prominent structures at the binding energy (E_B) of ~0.5 and 2–3 eV. These structures correspond to the bonding (*B*) and antibonding (*A*) final states due to the hybridization between the Ce $4f$ and other valence-band states. The bonding and antibonding states are described as the mixed states between the $4f^1\underline{L}$ and $4f^0$

TABLE I. The intensity (peak height) ratios of the peak *B* to *A* in the Ce $4f$ PES spectra.

	CePt*X*		CePd*X*	
X	$3d$-$4f$ RPES	$4d$-$4f$ RPES	$3d$-$4f$ RPES	$4d$-$4f$ RPES
P	3.1	1.2	2.3	1.2
As	2.0	1.1	3.1	1.0
Sb			1.9	0.7

configurations in the photoemission final states. Here, the *L* means a hole in the ligand band. The peak *B* is mainly composed of the $4f^1L$ component while the structure *A* is mainly composed of the $4f^0$ character. The $4f^1L$ final state arises from the transfer of an electron from the valence-band states to the $4f$ levels in order to screen the potential of the final state Ce $4f$ hole. Thus, the bonding (antibonding) peak is often called the ''well-screened'' (''poorly screened'') peak.

The peak structures *B* of both compounds are relatively enhanced in the $3d$-$4f$ RPES spectra compared to those in the $4d$-$4f$ RPES. On the other hand, the peak structures *A* in the $4d$-$4f$ RPES are relatively suppressed and weakened into shoulder structures in the $3d$-$4f$ RPES. These spectral line shapes indicate the difference of the hybridization of the Ce $4f$ states with the valence-band states between the bulk and surface. For the $3d$-$4f$ spectra, the intensity ratio of *B* to *A* of CePtP is larger than that of CePtAs as shown in Table I. This result shows a stronger hybridization strength in CePtP than in CePtAs.

The insets of Fig. 1 display the high-resolution RPES (HRPES) spectra in the vicinity of E_F taken at the Ce $3d$-$4f$ ($\Delta E \sim 100$ meV) and $4d$-$4f$ ($\Delta E \sim 50$ meV) thresholds. These results are tentatively normalized by the height at around 1.0 eV. The HRPES spectra have a weak hump and a peak (or shoulder) structure near E_F as shown by the vertical bars. These structures originate from the tail of the Kondo resonance ($4f_{5/2}$) and its spin-orbit sideband ($4f_{7/2}$). If the $3d$-$4f$ and $4d$-$4f$ HRPES spectra are compared, it is noticed that the difference is more prominent in CePtP than in CePtAs. This result indicates that the Kondo resonance develops more in the bulk of CePtP.

In order to understand the valence-band structures of CePt*X* (X=P,As), we present the non-$4f$ valence-band spectra taken at the resonance minimum, namely, at $h\nu \sim 875$ eV (shaded areas) and $h\nu \sim 114$ eV (dashed curves) in the right panels of Fig. 1. The weight of the resonance-minimum spectrum is much less than that of the resonance-maximum spectrum. For example, the intensity ratio of the resonance-maximum to resonance-minimum spectrum of CePtP is ~23 (3.4) for the $3d$-$4f$ ($4d$-$4f$) results. These resonance-minimum spectra of both compounds have rather similar shapes in regard to the main broad peak structures through 3 to 5 eV, the weak shoulder structure at around 6 eV and the hump structure near 1.5 eV along with the tendency of intensity decrease toward E_F. The similarity between the $3d$-$4f$ and $4d$-$4f$ results is ascribed to the strong Pt $5d$ contributions with the large photoionization cross section at these excitation energies. The finite density of states (DOS)

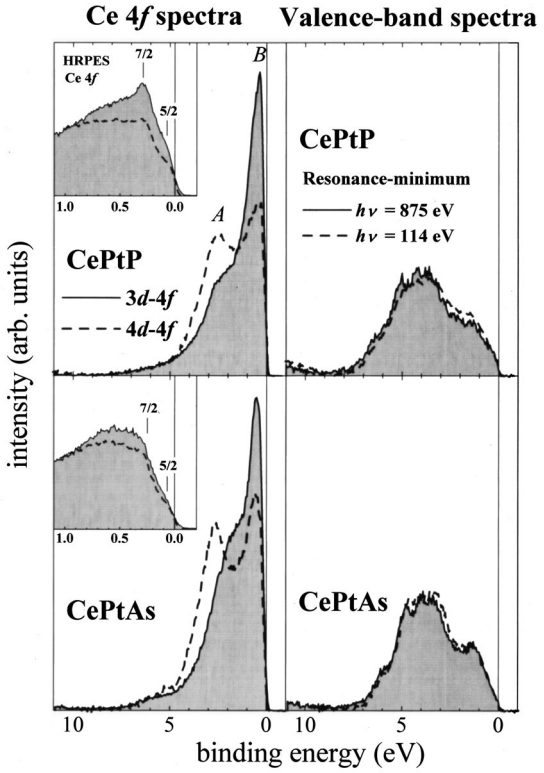

FIG. 1. Left panels: Ce $3d$-$4f$ resonance photoemission spectra (RPES) of CePt*X* (X=P,As) in comparison with the Ce $4d$-$4f$ RPES. The insets display high-resolution RPES (HRPES) spectra near E_F. Right panels: Comparison of the resonance-minimum spectra of CePt*X* taken at $h\nu \sim 875$ eV and 114 eV, representing the non-$4f$ valence-band structures. The spectral weight of the resonance-maximum to resonance-minimum spectra is arbitrary.

and the Fermi cutoff are clearly observed at E_F in the spectrum of CePtP, while the spectral intensity of CePtAs reduces almost linearly towards E_F and little DOS remains just at E_F. We consider that this larger DOS at E_F of CePtP causes the above-mentioned stronger hump and shoulder structures of the Ce $4f$ spectra in the HRPES spectra of CePtP (left upper inset).

Next, the $3d$-$4f$ and $4d$-$4f$ RPES spectra of CePd*X* (X=P,As,Sb) are shown in Fig. 2. All $4f$ spectra in the left panels are obtained by subtracting the non-$4f$ components. In addition, these spectra are normalized to the same area. The $4f$ components of CePd*X* consist of the two peak structures at around 3 eV (*A*) and 1 eV (*B*) as in the case of CePt*X*. In the whole valence-band region, peak *B* is much enhanced in the bulk-dominated $3d$-$4f$ spectra compared with the surface-dominated $4d$-$4f$ spectra, representing the stronger hybridization strength in the bulk. As summarized in Table I, the intensity ratios of *B* to *A* decrease from CePdP to CePdSb in the $4d$-$4f$ spectra, while the ratio is the largest in CePdAs in the $3d$-$4f$ spectra. These results reveal the significant differences in hybridization between the bulk and surface. The insets represent HRPES spectra near E_F. These HRPES spectra of CePd*X* have weak shoulder structures in the vicinity of E_F. These structures are derived likewise from the tail of the Kondo resonance ($4f_{5/2}$) and its spin-orbit partner ($4f_{7/2}$).

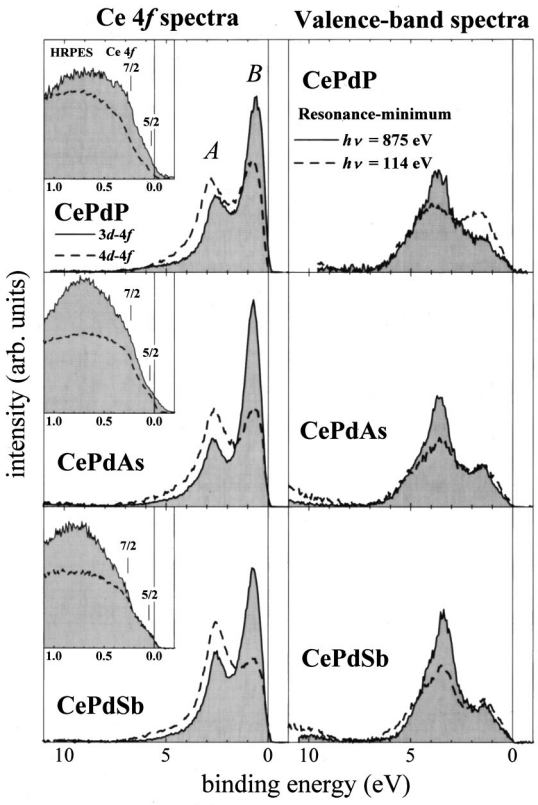

FIG. 2. Left panels: Comparison of the Ce $3d$-$4f$ RPES of CePdX (X=P,As,Sb) with the Ce $4d$-$4f$ RPES. The insets show HRPES spectra near E_F. Right panels: Non-$4f$ valence-band spectra of CePdX taken in the resonance-minimum regions ($3d$-$4f$:875 eV,$4d$-$4f$:114 eV). The spectral weight of the resonance-maximum to resonance-minimum spectra is arbitrary.

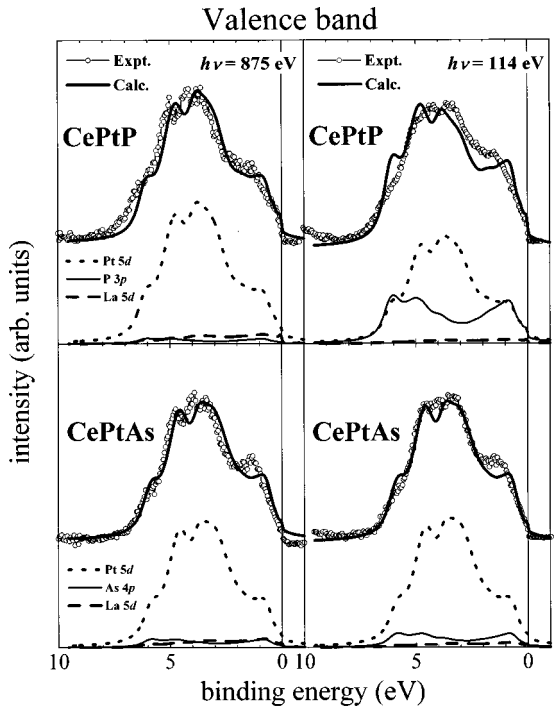

FIG. 3. Resonance-minimum spectra of CePtX (X=P,As) taken near the Ce $3d$ and $4d$ thresholds compared with the results of the band-structure calculation for LaPtX (X=P,As), which are broadened by a Gaussian and a Lorentzian function, considering the relative photoionization cross sections. See text for details.

The right panels of Fig. 2 show the resonance-minimum spectra of CePdX, corresponding to the non-$4f$ valence-band states. The spectral weight of the resonance-maximum to resonance-minimum spectrum of CePdP is ~21 (6.4) for the $3d$-$4f$ ($4d$-$4f$) results. We compare the resonance-minimum spectra in the $3d$-$4f$ (shaded areas) and the $4d$-$4f$ (dashed curves) excitation regions. The $3d$-$4f$ resonance-minimum spectra of CePdX are composed of the prominent peak structure at ~3.5 eV, the hump or peak structure at ~1.3 eV and the tail near 5 eV. The $4d$-$4f$ resonance-minimum spectra also have three corresponding structures, though the relative intensities are different. The broad structures clearly observed in the $4d$-$4f$ results at ~10 eV are originating from the pnictogen Xs states, whose intensity is very small in the $3d$-$4f$ results due to the relatively weak cross sections $\sigma_{Xs}/\sigma_{\mathrm{Pd}4d} \sim 0.06$ at 875 eV.[36] One notices that the intensities of the peaks near 3.5 eV relative to the 1.3-eV structures are noticeably stronger for the $3d$-$4f$ spectra than for the $4d$-$4f$ ones. This is because the photon energy $h\nu$ ~114 eV corresponds to the Cooper minimum for the Pd $4d$ states, which predominate near 3.5 eV.[36] The linearly decreasing intensities toward E_F and very low DOS at E_F are observed in both $3d$-$4f$ (bulk) and $4d$-$4f$ (surface) resonance-minimum spectra, suggesting that the hybridization strengths of the Ce $4f$ states with these valence-band states are very weak near E_F. This situation explains the rather weak $4f$-derived shoulder structures near E_F in both bulk- and surface-sensitive HRPES spectra (left insets).

B. Comparison of resonance-minimum spectra with band-structure calculations

In Figs. 3 and 4 are compared the experimental results for CePtX and CePdX with the results of the band-structure calculations for isostructural La compounds LaPtX and LaPdX performed by a full-potential linear augmented plane-wave method.[26,27,37,38] The calculated results are convoluted by a Lorentzian function, originating from the lifetime of the photoemission final states, and then by a Gaussian function with a fixed FWHM of 100 meV corresponding to the experimental resolution.[39] Referring to the previous report based on the self-energy method,[40] we approximate the width of the Lorentzian as the square of the binding energy (eV) up to the maximum FWHM value of 0.25 eV in the high-energy region. We also consider the photoionization cross section σ for each orbital at the excitation energies of 875 eV and 114 eV.[36] We summarize the convoluted partial density of states (PDOS) of the primary orbital for each element at the bottom of each panel of Figs. 3 and 4. The thick solid curves stand for the sum of these three PDOS curves. In Fig. 3 for CePtX, we compare the non-$4f$ valence-band spectra (open circles) taken at the $3d$-$4f$ (left panels) and $4d$-$4f$ (right panels) resonance-minimum excitation energies with the results of band-structure calculations for LaPtX.[26] In the left panels of

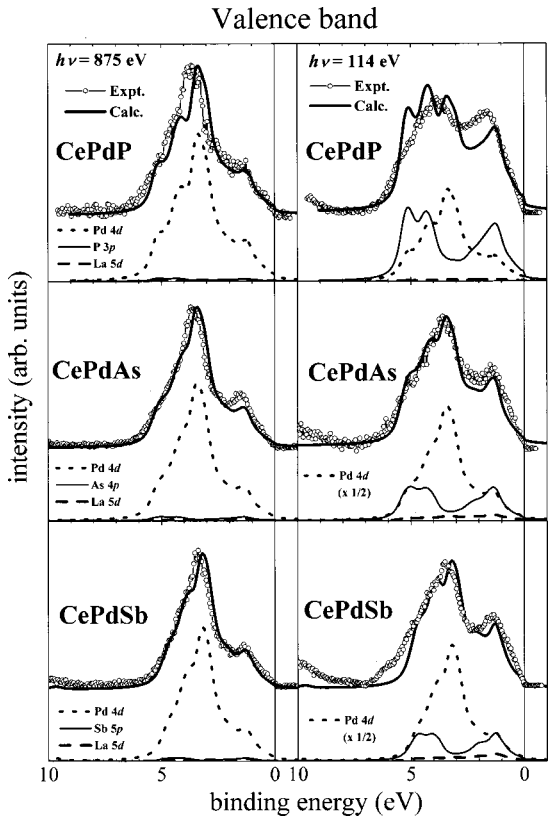

FIG. 4. Comparison of the $3d$-$4f$ and $4d$-$4f$ resonance-minimum spectra of CePdX (X=P,As,Sb) with the partial density of states (PDOS) obtained by the band-structure calculation for LaPdX (X=P,As,Sb). The PDOS are convoluted by a Gaussian and a Lorentzian function, taking the photoionization cross sections into account.

Fig. 3, the calculated results (thick solid curves) well reproduce the $3d$-$4f$ experimental results. The Pt $5d$ contribution is dominant in the whole valence-band region because the photoionization cross section ratios of the Pt $5d$ to other orbitals are $\sigma_{\mathrm{Pt}5d}/\sigma_{\mathrm{La}5d}\sim 19$ and $\sigma_{\mathrm{Pt}5d}/\sigma_{Xp}\sim 10-20$ at $h\nu \sim 875$ eV.[36]

The right panels of Fig. 3 compare the band-structure calculations[26] with the surface-sensitive resonance-minimum spectra (open circles) taken at $h\nu\sim 114$ eV. At this photon energy, $\sigma_{\mathrm{Pt}5d}/\sigma_{\mathrm{La}5d}\sim 40$ and $\sigma_{\mathrm{Pt}5d}/\sigma_{Xp}\sim 6-8$ for X=As and Sb, then the Pt $5d$ contribution is still dominant in these valence-band spectra. For the case of CePtP, however, $\sigma_{\mathrm{Pt}5d}/\sigma_{\mathrm{P}3p}\sim 1.6$.[36] The calculated results represented by the thick solid curves well reproduce the experimental results for these materials. For CePtP, the contribution of the P $3p$ component to the structures at around 1.5 eV and 6.0 eV are as large as the contribution from the Pt $5d$ component. Thus, we consider that the structures at ~6.0 eV are derived from the bonding states between the Pt $5d$ and P $3p$ states and the shoulder structures at around 1.5 eV arise from their antibonding states. The main peak structures ranging from 3 to 4 eV are originating from the nonbonding states of the Pt $5d$ states. The similar interpretation is applicable to the case of CePtAs. It is thus confirmed that the band-structure calculation for LaPtX well describes the valence-band spectra derived from the resonance-minimum spectra by taking the photoionization cross sections into account. Some discrepancies between the experimental and calculated results, particularly in the $4d$-$4f$ energy region, may come from the surface effect. However, the surface effect is less obvious in the valence-band spectra of CePtX than in the Ce $4f$ spectra.

Figure 4 likewise compares the PDOS obtained by the band-structure calculations for LaPdX[26,27] with the experimental non-$4f$ valence-band spectra of CePdX. In the $3d$-$4f$ resonance minimum spectra displayed in the left panels of Fig. 4, the Pd $4d$ contributions are much stronger than other components in the whole valence-band region because of the large cross section of the Pd $4d$ states in this energy region ($h\nu\sim 875$ eV: $\sigma_{\mathrm{Pd}4d}/\sigma_{Xp}\sim 20$ and $\sigma_{\mathrm{Pd}4d}/\sigma_{\mathrm{La}5d}\sim 30$).[36] The thick solid curves obtained by adding the PDOS components well reproduce the experimental spectra, namely, the main peak at around 3.5 eV, a shoulder at around 5.0 eV, and a hump or peak structure at around 1.3 eV. It is thus found that the $3d$-$4f$ resonance-minimum spectra for CePdX are predominantly composed of the Pd $4d$ states.

The right panels of Fig. 4 display the PDOS of LaPdX and the relatively surface-sensitive valence-band spectra for CePdX taken at $h\nu\sim 114$ eV. This excitation photon energy corresponds to the Cooper minimum of the Pd $4d$ states. Thus, the relative cross section ratios of the Pd $4d$ states to others are $\sigma_{\mathrm{Pd}4d}/\sigma_{Xp}\sim 1-4$ and $\sigma_{\mathrm{Pd}4d}/\sigma_{\mathrm{La}5d}\sim 20$.[36] Here, the experimental spectra are not well reproduced by the calculation, in particular, in the case of CePdP. However, by assuming relative suppression of $\sigma_{\mathrm{Pd}4d}$ in the Cooper minimum region down to 1/2 of the predicted value,[36] the observed spectra of CePdAs and CePdSb are well reproduced. The deviation of σ from the predicted value[36] is quite possible in the Cooper minimum region in solids. Thus the band-structure calculations almost reproduce the valence-band spectra of CePdAs and CePdSb by considering the $h\nu$ dependence of the photoionization cross sections. The structures at around 1.3 and 5.0 eV correspond to the p-d antibonding and bonding states. Some noticeable differences remain between the calculated DOS and the experimental spectra in the case of CePdP for both $4d$-$4f$ and $3d$-$4f$ resonance minimum spectra. The energy separation between the bonding and antibonding parts located at around 1.3 and 4–5 eV seems to be too large in the calculation. This may be arising from the ignorance of the final-state hybridization of the valence bands (with the Ce $4f$ states) in the band-structure calculation for La system. In this respect, the hybridization strength $\rho V^2(E)$ of CePdP is the strongest near 2.0 eV. In this system of CePdX, the surface effect is again less obvious than for the Ce $4f$ spectra.

C. Analyses of the Ce $4f$ spectra

In order to discuss the differences of the Ce $4f$ electronic structures among CeMX series as well as between the bulk and surface, we have calculated the Ce $4f$ spectra by the NCA method within SIAM. The surface/bulk intensity ratio I_s/I_b is given by $\exp[d/(\lambda\cos\theta)]-1$. Here, d means the thickness of the surface layer and λ is the mean-free path of the photoelectrons as a function of the kinetic energy. The

values of λ were determined by using the formula for the inelastic mean-free path proposed by Tanuma, Powell, and Penn[41] and are estimated to be about 17 and 5 Å at the Ce $3d$-$4f$ and Ce $4d$-$4f$ RPES, respectively. The value of d is assumed to be the nearest neighbor Ce-Ce distance. The values of the I_s/I_b are approximately 1.3 and 0.3 for the Ce $4d$-$4f$ and Ce $3d$-$4f$ RPES, respectively. We choose the parameters so as to reproduce both the peak positions and the spectral shapes by a sum of surface and bulk components with the given I_s/I_b weight. In our previous work,[34] we have found that the resonance-minimum spectra do not faithfully reflect the energy dependence of the strength of hybridization, $\rho V^2(E)$, with the Ce $4f$ states and that the proper $\rho V^2(E)$ for CeMX emphasize the antibonding states between the Md and Xp states.

The solid (dashed) lines in Fig. 5(a) show the energy dependence of $\rho V^2(E)$ and the bare $4f_{5/2}$ level energies ϵ_f used for the bulk (surface) $4f$ spectral calculation of CePtX. The PDOS of the Xp states obtained by the band-structure calculations for LaPtX (X=P,As) are also reproduced in Fig. 5(a).[26] These $\rho V^2(E)$ emphasize the hybridization of the Ce $4f$ states with the antibonding states between the Pt $5d$ and pnictogen Xp states at around 1.3 eV as indicated by the dotted lines. The $\rho V^2(E)$ are assumed to decrease linearly toward E_F according to the experimental spectral features. Considering the finite DOS of the conduction-band states, we also assume constant DOS above E_F with $\rho V^2(E_F)=9.5$ and 7.5 meV for CePtP and CePtAs, respectively. We set ϵ_f to 1.6 (2.7) and 1.7 (2.5) eV for the bulk (surface) spectra of CePtP and CePtAs, respectively. Here, the spin-orbit splitting of the Ce $4f$ states is set to 0.27 eV for both compounds.

The left panels of Fig. 5(b) show the experimental $3d$-$4f$ RPES spectra (open circles) for CePtX and the calculated results (thick solid curves) that are the sum of the bulk and surface components with the estimated ratios of $I_s/I_b \sim 0.28$ for both CePtP and CePtAs. The calculated curves semiquantitatively reproduce the $3d$-$4f$ experimental results. It is noticed that the bulk contributions are dominant in the whole energy region.

On the other hand, the surface-sensitive $4d$-$4f$ spectra (open circles) are compared in the right panels with the NCA calculation (thick solid curves), the sum of the surface and bulk spectra with the intensity ratios of $I_s/I_b \sim 1.35$ and 1.31 for CePtP and CePtAs, respectively. The NCA calculation also reproduces the experimental results. It is thus recognized in the $4d$-$4f$ RPES that the surface Ce $4f$ components strongly influence the spectral shape in the high-binding-energy region near 2.5 eV. As shown in Fig. 5(a), the surface effect is mostly represented by the shift of the bare Ce $4f$ levels.

Some quantitative discrepancies between the experimental and calculated results are seen in Fig. 5(b). For example, the surface contribution near 2 eV in the calculated result is larger than the experimental $3d$-$4f$ result in CePtP whereas it is comparable to the $4d$-$4f$ RPES result. In addition, the energy position of the antibonding peak in the calculated $4d$-$4f$ curve in CePtAs is lower (smaller) than that in the experimental result. These discrepancies near the antibonding peaks suggest a more complicated surface contribution, for example, the possibility of the contribution of the second surface layer, which has different electronic structures compared with the first surface layer. However, such a discussion is much more difficult than the case of Yb compounds (where the contribution of the second surface layer is clearly observed[42]) and is beyond the discussion of the present paper.

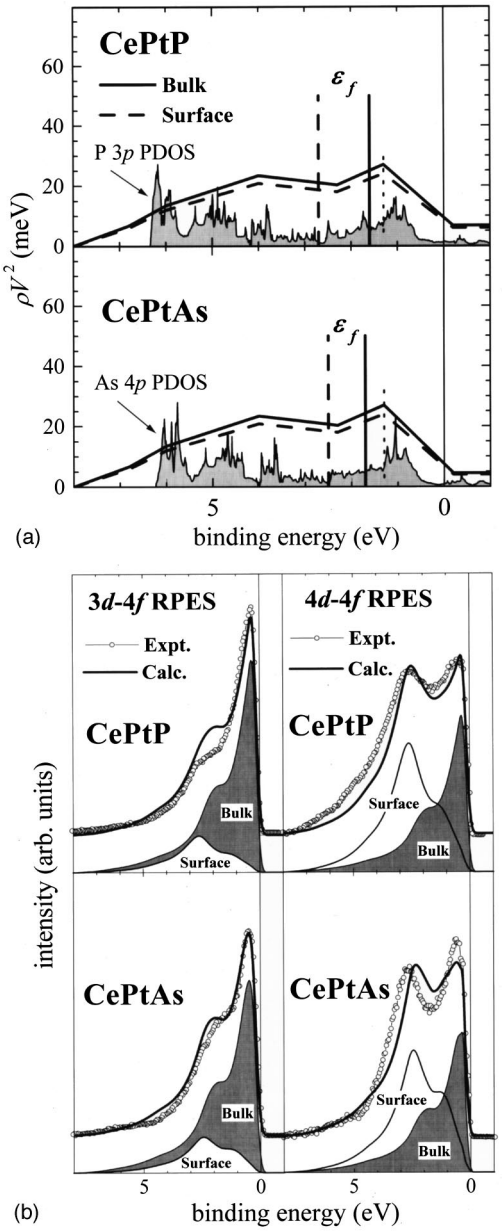

FIG. 5. (a) PDOS of the pnictogen Xp states of CePtX (X=P,As) are compared with the optimized $\rho V^2(E)$ employed in the NCA calculation and represented by the solid (dashed) lines for the bulk (surface) component. (b) Comparison of the $3d$-$4f$ (left panels) and $4d$-$4f$ RPES (right panels) spectra with the results of NCA calculations.

Similar results are shown for CePdX (X=P,As,Sb) in Figs. 6(a) and 6(b). We calculate the bulk (surface) $4f$ spectrum with ϵ_f of 1.7 (2.7), 1.6 (2.7), and 1.7 (2.7) eV for

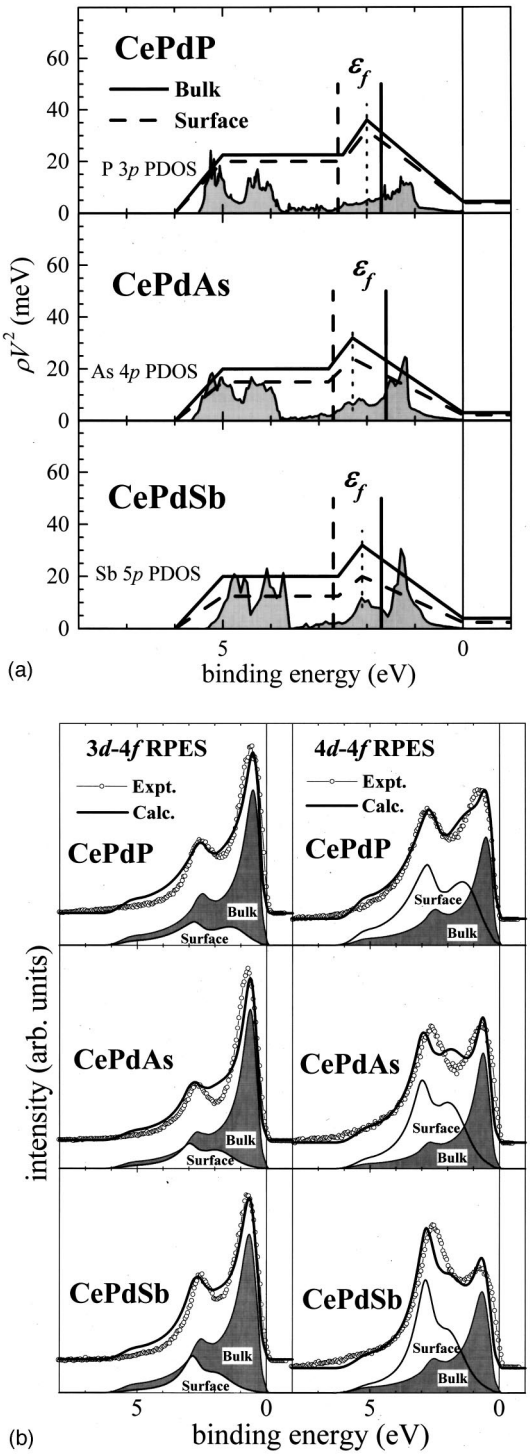

FIG. 6. (a) Comparison of the optimized $\rho V^2(E)$ and other parameters used in the NCA calculation with the PDOS of the pnictogen Xp states. (b) Ce $4f$ spectra of CePdX (X=P,As,Sb) taken by means of the $3d$-$4f$ (left panels) and $4d$-$4f$ (right panels) RPES are compared with the results of NCA calculation.

CePdP, CePdAs, and CePdSb, respectively. The spin-orbit splitting of the Ce $4f$ states is set to 0.27 eV. The energies of the maximum of $\rho V^2(E)$, ϵ_p, indicated by the dotted lines are 2.0, 2.3, and 2.1 eV for CePdP, CePdAs, and CePdSb, respectively.

In Fig. 6(b), the NCA calculations (thick solid curves) are compared with the experimental $4f$ spectra (open circles). For the $3d$-$4f$ RPES, the surface/bulk intensity ratios I_s/I_b for CePdP, CePdAs, and CePdSb are evaluated as 0.27, 0.27, and 0.26, respectively. The calculated results well explain the $3d$-$4f$ RPES spectra as shown in the left panels. The bulk contributions are predominant in the whole energy range.

The right panels compare the calculated results with the surface-sensitive $4d$-$4f$ RPES spectra. The experimental spectra are fairly reproduced by the calculated curves with $I_s/I_b \sim 1.33$ (CePdP), 1.29 (CePdAs), and 1.26 (CePdSb), respectively. Generally speaking, the spectral differences among these compounds are explained by the material dependence of $\rho V^2(E)$, its maximum ϵ_p, and the bare Ce $4f$ level energy ϵ_f, by means of SIAM. Here again, the surface effect is mainly described by the shift of the bare $4f$ level as shown in Fig. 6(a). However, still some discrepancies are seen near 3 eV in the $4d$-$4f$ RPES of CePdAs and CePdSb as in CePtAs. In addition, a hump near 2 eV in the calculated result of CePdAs is not observed in the $4d$-$4f$ RPES result. A corresponding discrepancy between the calculated and experimental spectra is also recognized in the $3d$-$4f$ RPES in CePdAs. Such discrepancies may be resulting from the possible overestimation of $\rho V^2(E)$ in CePdAs near 2.3 eV. There may be still some rooms to improve the fitting by employing more sophisticated shapes of $\rho V^2(E)$. Such a procedure is, however, beyond the scope of the present paper.

D. Discussion

We compare the employed parameters in the NCA analyses for the present samples in Table II. In the first place, the bare $4f_{5/2}$ level energies ϵ_f, which represent the energy position before the Ce $4f$ states are hybridized with other valence bands, are almost the same between CePtX and CePdX. The ϵ_f of CeMX are estimated to be 1.6–1.7 (2.5–2.7) eV for the bulk (surface). This result shows that these materials have the similar surface core-level shift of $\sim$1 eV and then the difference of ϵ_f causes the spectral changes between the bulk and surface. Second, the maximum positions ϵ_p of the $\rho V^2(E)$ show clear sample dependence, namely, the ϵ_p are 1.3 eV and 2.0–2.3 eV for CePtX and CePdX, respectively.

In the case of CePtX, for example, the PDOS of the Xp states reproduced in Fig. 5(a) consist roughly of three parts. The structures from 6.3 to 4.2 eV, mainly corresponding to the p-d bonding states, and the structures from 2.7 eV to E_F are mostly derived from the p-d antibonding states. In the region from 4.2 to 2.7 eV with the very low PDOS of the p states, the very high PDOS of the Pt $5d$ nonbonding states are located as shown in Fig. 3. The employed $\rho V^2(E)$ is much different from the PDOS of the Pt $5d$ states. Therefore, the Xp states rather than the Pt $5d$ states are thought to strongly influence the hybridization with the Ce $4f$ states through the p-d antibonding states. Considering the crystal

TABLE II. Parameters used in the NCA calculation for the bulk and surface components. The $4f$ electron number n_f is obtained from this analysis.

	Bulk				
	ϵ_f (eV)	ϵ_p (eV)[a]	$\rho V^2(E_F)$[b] (meV)	Δ (meV)[c]	n_f
CePtP	1.6	1.3	9.5	52	0.992
CePtAs	1.7	1.3	7.5	52	0.995
CePdP	1.7	2.0	4.5	64	0.997
CePdAs	1.6	2.3	3.2	56	0.997
CePdSb	1.7	2.1	4.0	57	0.997
	Surface				
	ϵ_f (eV)	ϵ_p (eV)[a]	$\rho V^2(E_F)$[b] (meV)	Δ (meV)[c]	n_f
CePtP	2.7	1.3	8.4	47	0.996
CePtAs	2.5	1.3	6.7	46	0.996
CePdP	2.7	2.0	4.0	57	0.998
CePdAs	2.7	2.3	2.4	42	0.998
CePdSb	2.7	2.1	2.5	36	0.998

[a]Maximum position of the energy distribution $\rho V^2(E)$.
[b]The values of $\rho V^2(E)$ at the Fermi level.
[c]The average of the hybridization strength defined as the following: $\Delta = \pi \int_0^B \rho V^2(E)/B dE$ (B represents the valence-band width in eV).

structures of CePtX, the Ce atoms are far outside the Pt-X plane. Namely, the hybridization between the Ce $4f$ and Xp_z states is stronger than that between the Ce $4f$ and other states. The ϵ_p of the employed $\rho V^2(E)$ in CePtX indicates a particular region with the large Xp_z component in the p-d antibonding states.

Likewise the p-f mixing is more important than the d-f mixing in CePdX because the used $\rho V^2(E)$ does not reflect the PDOS of the Pd $4d$ states as shown in Fig. 4. Again, due to the crystal structure, the p_z component of the Xp states should play an important role in the hybridization of the Ce $4f$ states with the p-d antibonding states. In each PDOS of the Xp states in Fig. 6(a), we can recognize a few structures, namely, two broad peak or hump structures at around 1.3 eV and 2.1 eV (in the antibonding states of the p-d mixed states), the considerably low DOS near 3 eV, and the two-peak structures at around 4 and 5 eV (in the bonding states). When the PDOS are compared with the used $\rho V^2(E)$, each ϵ_p corresponds quantitatively to the hump near 2 eV in the antibonding states. Therefore, the hump structure of the p-d mixed antibonding states should contain the large p_z contribution, supported by the results of the band-structure calculations.[26]

Third, the $\rho V^2(E_F)$ in Table II represents the hybridization strength just at E_F. The parameters of 7–10 meV in CePtX are larger than those of 3–5 meV in CePdX for the bulk. This parameter is directly related to the spectral weight of the shoulder structure in the HRPES spectra near E_F. The $\rho V^2(E_F)$ of CePtP is the largest among the present CeMX series in both the bulk and surface, providing the enhanced structures near E_F in the HRPES spectrum shown in the inset of Fig. 1. The $\rho V^2(E_F)$ should be related to the Kondo temperature and the effective mass of the conduction electrons.

Although the average bulk hybridization strengths Δ for both CePtP and CePtAs are evaluated as 52 meV, the intensity ratio of the bulk peak B to A of CePtP is noticeably larger than that of CePtAs as seen in the first column of Table I. On the other hand, the Δ for the bulk components of CePdP ($\Delta = 64$ meV), CePdAs ($\Delta = 56$ meV), and CePdSb ($\Delta = 57$ meV) have a trend of being different from the intensity ratios of the peak B to A. Namely, the bulk $4f$ spectrum of CePdAs with the largest B/A ratio is reproduced by using the smallest Δ among CePdX. In contrast to a simplified prediction, the average hybridization strength Δ is not directly related to the intensity ratio of the peak B to A in the Ce $4f$ spectra. Thus, we need to consider the realistic energy dependence of the hybridization strength $\rho V^2(E)$ in quantitatively reproducing the Ce $4f$ spectra.

The $4f$ spectral changes in CePtX depend mainly upon the ϵ_f and $\rho V^2(E_F)$. The ϵ_f sensitively varies the intensity ratios of B/A in CePtX while $\rho V^2(E_F)$ influences the shoulder structures in the HRPES spectra near E_F. As for CePdX, it is understood that the difference in energy separation between the ϵ_p and ϵ_f further influences the B/A ratios of the $4f$ spectra. On the other hand, the spectral changes by the substitution of Pt by Pd arise from the whole line shape of $\rho V^2(E)$ and its maximum positions ϵ_p as discussed above.

IV. CONCLUSION

We have performed Ce $3d$-$4f$ and $4d$-$4f$ RPES measurements for the ternary Ce pnictide CeMX (M=Pd,Pt,X=P,As,Sb). The intensity ratios of the bonding to antibonding components in the bulk $4f$ spectra are much higher than those in the surface-sensitive $4d$-$4f$ RPES spectra. The high-resolution $4f$ spectra of CeMX show the weak shoulder structures near E_F corresponding to the tail of the Kondo resonance and its spin-orbit splitting sideband. The characteristic spectral features originate from the rather small DOS of the valence-band states near E_F.

From the comparison of the non-$4f$ valence-band spectra with the results of the band-structure calculations of isostructural LaMX (M=Pd,Pt,X=P,As,Sb), we find that the valence-band spectra are well described by the PDOS of LaMX by taking the relative photoionization cross sections into account. In contrast with the clear difference between the surface and bulk Ce $4f$ spectra, the non-$4f$ valence-band spectra do not noticeably depend upon the surface sensitivity in the present system with low T_K.

The NCA calculation shows that the energy dependence $\rho V^2(E)$ employed for explaining the Ce $4f$ spectra of CeMX emphasizes the hybridization with the antibonding part of the p-d mixed states. It is also found that the bare $4f$ level shift is the most important factor in explaining the difference between the surface and bulk spectra. It is found that the hybridization strengths of the Ce $4f$ states in CePtX are the strongest in the region near 1.3 eV whereas the Ce $4f$ states of CePdX are strongly hybridized with the hump structure at around 2.1 eV. It is necessary to properly consider the energy dependence of the hybridization strength $\rho V^2(E)$ instead of the average hybridization strength Δ in reproducing the Ce $4f$ PES spectra.

ACKNOWLEDGMENTS

The authors are grateful to the staff of SPring-8 and PF, especially to T. Nakatani, E. Shigemasa, and T. Saitoh, for supporting the experiments. We are much obliged to O. Sakai and R. Takayama for their kind instruction on the NCA calculation. We are much obliged to H. Osaka and T. Suzuki for providing some samples. We would like to thank H. Ishii, M. Kotsugi, S. Ueda, K. Matsuda, T. Ushida, K. Kusuda, and T. Satonaka for their technical help. This work was supported by a Grant-in-Aid for COE Research (10CE2004) of the Ministry of Education, Culture, Sports, Science and Technology, Japan. The $3d$-$4f$ RPES measurements were performed with the approval of the Japan Synchrotron Radiation Research Institute (JASRI) (Proposal Nos. 1997B1043-NS-np and 1999A0315-NS-np). The Ce $4d$-$4f$ RPES measurements were carried out under the approval of the PF Program Advisory Committee (Proposal Nos. 92S002, 97G298, and 99G150).

*Present address: Department of Physics, Nagoya University, Nagoya 464-8602, Japan.

[1] J. C. Fuggle, F. U. Hillebrecht, Z. Zolnierek, R. Lässer, Ch. Freiburg, O. Gunnarsson, and K. Schöhammer, Phys. Rev. B **27**, 7330 (1983).

[2] J. W. Allen, S.-J. Oh, O. Gunnarsson, K. Schönhammer, M. B. Maple, M. S. Torikachvili, and I. Lindau, Adv. Phys. **35**, 275 (1986).

[3] A. Kakizaki, A. Harasawa, T. Ishii, T. Kashiwakura, A. Kamata, and S. Kunii, J. Phys. Soc. Jpn. **64**, 302 (1995).

[4] M. Tsunekawa, S. Suga, A. Kimura, T. Matsushita, T. Muro, S. Ueda, H. Daimon, S. Imada, T. Nakatani, Y. Saitoh, T. Iwasaki, A. Sekiyama, A. Fujimori, H. Ishii, T. Miyahara, T. Hanyu, H. Namatame, M. Taniguchi, E. Shigemasa, O. Sakai, R. Takayama, R. Settai, H. Azuma, and Y. Onuki, Solid State Commun. **103**, 659 (1997).

[5] C. Laubschat, E. Weschke, C. Holtz, M. Domke, O. Strebel, and G. Kaindl, Phys. Rev. Lett. **65**, 1639 (1990).

[6] E. Weschke, C. Laubschat, T. Simmons, M. Domke, O. Strebel, and G. Kaindl, Phys. Rev. B **44**, 8304 (1991).

[7] C. Laubschat, E. Weschke, M. Domke, C. T. Simmons, and G. Kaindl, Surf. Sci. **269/270**, 605 (1992).

[8] G. Chiaia, P. Vavassori, L. Duò, L. Braicovich, M. Qvarford, and I. Lindau, Surf. Sci. **331–333**, 1229 (1995).

[9] L. Duò, Surf. Sci. Rep. **32**, 233 (1998).

[10] H.-D. Kim, O. Tjernberg, G. Chiaia, H. Kumigashira, T. Takahashi, L. Duò, O. Sakai, M. Kasaya, and I. Lindau, Phys. Rev. B **56**, 1620 (1997).

[11] L. Duò, Surf. Sci. **377–379**, 160 (1997).

[12] L. Duò, S. De Rossi, P. Vavassori, F. Ciccacci, G. L. Olcese, G. Chiaia, and I. Lindau, Phys. Rev. B **54**, R17363 (1996).

[13] Y. Saitoh, H. Kimura, Y. Suzuki, T. Nakatani, T. Matsushita, T. Muro, T. Miyahara, M. Fujisawa, K. Soda, S. Ueda, H. Harada, M. Kotsugi, A. Sekiyama, and S. Suga, Rev. Sci. Instrum. **71**, 3254 (2000).

[14] A. Sekiyama, T. Iwasaki, K. Matsuda, Y. Saitoh, Y. Onuki, and S. Suga, Nature (London) **403**, 396 (2000).

[15] A. Sekiyama, K. Kadono, K. Matsuda, T. Iwasaki, S. Ueda, S. Imada, S. Suga, R. Settai, H. Azuma, Y. Onuki, and Y. Saitoh, J. Phys. Soc. Jpn. **69**, 2771 (2000).

[16] S. Suga, Nucl. Instrum. Methods Phys. Res. A **467–468**, 1388 (2001).

[17] A. Sekiyama and S. Suga (unpublished).

[18] H. Kumigashira, S.-H. Yang, T. Yokoya, A. Chainani, T. Takahashi, A. Uesawa, and T. Suzuki, Phys. Rev. B **55**, 3355 (1997).

[19] A. Franciosi, J. H. Weaver, N. Mårtensson, and M. Croft, Phys. Rev. B **24**, 3651 (1981).

[20] A. Fujimori, M. Grioni, J. J. Joyce, and J. H. Weaver, Phys. Rev. B **31**, 8291 (1985).

[21] S. Yoshii, M. Kasaya, H. Osaka, and H. Suzuki, Jpn. J. Appl. Phys. Series 11, 132 (1999).

[22] S. Yoshii, H. Suzuki, D. Tazawa, and M. Kasaya, J. Phys. Soc. Jpn. **66**, 2569 (1997).

[23] S. Yoshii, H. Suzuki, T. Miyazaki, and M. Kasaya, J. Magn. Magn. Mater. **177–181**, 427 (1998).

[24] K. Katoh, A. Ochiai, and T. Suzuki, Physica B **223&224**, 340 (1996).

[25] S. K. Malik and D. T. Adroja, Phys. Rev. B **43**, 6295 (1991).

[26] K. Takegahara and H. Harima (unpublished).

[27] M. Akuura and T. Oguchi (unpublished).

[28] N. E. Bickers, D. L. Cox, and J. W. Wilkins, Phys. Rev. B **36**, 2036 (1987).

[29] N. E. Bickers, Rev. Mod. Phys. **59**, 845 (1987).

[30] Y. Kuramoto, Z. Phys. B: Condens. Matter **53**, 37 (1983).

[31] P. W. Anderson, Phys. Rev. **124**, 41 (1961).

[32] O. Gunnarsson and K. Schönhammer, in *Handbook on the Physics and Chemistry of Rare Earths*, edited by K. A. Gschneidner, L. Eyring, and S. Hüfner (Elsevier, Amsterdam, 1987), Vol. 10, pp. 103–163.

[33] A. Yagishita, T. Hayaishi, T. Kikuchi, and E. Shigemasa, Nucl. Instrum. Methods Phys. Res. A **306**, 578 (1991).

[34] T. Iwasaki, S. Suga, S. Imada, A. Sekiyama, K. Matsuda, M. Kotsugi, K.-S. An, T. Muro, S. Ueda, T. Matsushita, Y. Saitoh, T. Nakatani, H. Ishii, O. Sakai, R. Takayama, T. Suzuki, T. Oguchi, K. Katoh, and A. Ochiai, Phys. Rev. B **61**, 4621 (2000).

[35] A. Sekiyama, S. Suga, T. Iwasaki, S. Ueda, S. Imada, Y. Saitoh, T. Yoshino, D. T. Adroja, and T. Takabatake, J. Electron Spectrosc. Relat. Phenom. **114–116**, 699 (2001).

[36] J. J. Yeh and I. Lindau, At. Data Nucl. Data Tables **32**, 1 (1985).

[37] E. Wimmer, H. Krakauer, M. Weinert, and A. J. Freeman, Phys. Rev. B **24**, 864 (1981).

[38] R. Settai, Y. Yoshida, A. Yamaguchi, Y. Onuki, S. Yoshii, M. Kasaya, H. Harima, and K. Takegahara, J. Phys. Soc. Jpn. **68**, 3615 (1999).

[39] At each E_B, a Lorentzian contribution is considered, whose FWHM is assumed to increase with E_B reflecting the shorter lifetime.

[40] A. Sekiyama, T. Susaki, A. Fujimori, T. Sasaki, N. Toyota, T. Kondo, G. Saito, M. Tsunekara, T. Iwasaki, T. Muro, T. Matsushita, S. Suga, H. Ishii, and T. Miyahara, Phys. Rev. B **56**, 9082 (1997).

[41] S. Tanuma, C. J. Powell, and D. R. Penn, Surf. Sci. **192**, L849 (1987).

[42] S. Suga (unpublished).